Chemical Science

ROYAL SOCIETY OF CHEMISTRY

REVIEW

View Article Online
View Journal | View Issue

Cite this: *Chem. Sci.*, 2021, **12**, 6488

Recent advances of AIE light-up probes for photodynamic therapy

Shanshan Liu,[a] Guangxue Feng,*[a] Ben Zhong Tang *[ab] and Bin Liu *[c]

Received 5th January 2021
Accepted 22nd February 2021

DOI: 10.1039/d1sc00045d

rsc.li/chemical-science

As a new non-invasive treatment method, photodynamic therapy (PDT) has attracted great attention in biomedical applications. The advantages of possessing fluorescence for photosensitizers have made it possible to combine imaging and diagnosis together with PDT. The unique features of aggregation-induced emission (AIE) fluorogens provide new opportunities for facile design of light-up probes with high signal-to-noise ratios and improved theranostic accuracy and efficacy for image-guided PDT. In this review, we summarize the recent advances of AIE light-up probes for PDT. The strategies and principles to design AIE photosensitizers and light-up probes are firstly introduced. The application of AIE light-up probes in photodynamic antitumor and antibacterial applications is further elaborated in detail, from binding/targeting-mediated, reaction-mediated, and external stimuli-mediated light-up aspects. The challenges and future perspectives of AIE light-up probes in the PDT field are also presented with the hope to encourage more promising developments of AIE materials for phototheranostic applications and translational research.

1. Introduction

Photodynamic therapy (PDT) as a photo-regulated treatment modality for cancers and other diseases has received widespread attention during the past few decades.[1] PDT involves the incorporation of the disease-site accumulated photosensitizers, light and oxygen to generate toxic reactive oxygen species (ROS) to kill cancer cells and destroy disease tissues.[2] Under light irradiation, the photosensitizer could be excited to its singlet excited state, from which state it could generate fluorescence *via* a radiative pathway or undergo intersystem crossing (ISC) to the triplet state and further react with the surrounding oxygen or substrates to generate ROS.[3] As a highly toxic substance, ROS can trigger the death of disease tissues by causing cell apoptosis or necrosis, destroying blood vessels, and stimulating an immune response. Moreover, the short action radius and lifetime of ROS also help to constrain the damage only to cancer cells or microbes that receive specific light irradiation, which minimizes the side effect on normal tissues and largely improves the therapeutic accuracy. Therefore, PDT has been recognized as a non-invasive disease treatment modality.[4]

As the main part of PDT, photosensitizers play vitally important roles not only in generating ROS but also in guiding the light irradiation locations *via* their fluorescence signals. However, the improvement of the photosensitization ability and imaging sensitivity of photosensitizers remains a challenge for PDT. One of the main reasons is that most conventional photosensitizers (such as porphyrins, rose bengal, *etc.*) have planar structures, which suffer from the aggregation-caused quenching (ACQ) effect due to their strong π–π interaction in aggregates.[5] This not only leads to reduced fluorescence signals but also causes compromised photosensitization at high concentrations or aggregate states after photosensitizers accumulate at disease tissues. Another reason is that the always-on fluorescence signal of conventional photosensitizers undermines the imaging sensitivity, making it difficult to distinguish the targets from these off-target background signals and to precisely manipulate the light irradiation area.[6,7] Therefore, developing new photosensitizers with improved photosensitization ability and specific fluorescence light-up capability is highly desired.

The discovery and development of aggregation-induced emission (AIE) fluorogens provide new opportunities for fluorescence imaging and PDT. The concept of AIE was first coined in 2001, and refers to a unique phenomenon that fluorogens are not emissive in the molecular state but show largely intensified fluorescence in the aggregate or solid state.[8] AIE fluorogens (AIEgens) usually possess propeller structures, and the free molecular motions in the molecular state dissipate excited energy *via* nonradiative pathways, while molecular aggregation suppresses such nonradiative decay pathways and activates the

[a]*State Key Laboratory of Luminescent Materials and Devices, Guangdong Provincial Key Laboratory of Luminescence from Molecular Aggregates, AIE Institute, School of Materials Science and Engineering, South China University of Technology, Guangzhou, 510640, China. E-mail: fenggx@scut.edu.cn; tangbenz@ust.hk*

[b]*Department of Chemistry, The Hong Kong University of Science & Technology (HKUST), Clear Water Bay, Kowloon, Hong Kong, China*

[c]*Department of Chemical and Biomolecular Engineering, National University of Singapore, 4 Engineering Drive 4, Singapore, 117585, Singapore. E-mail: cheliub@nus.edu.sg*

radiative decay pathway to emit fluorescence strongly.[9] The unique optical properties of AIEgens make them the ideal candidates for developing light-up probes *via* target-mediated aggregate formation or restriction of intramolecular motions (RIM). So far, various AIE probes have been developed for biological and biomedical applications, such as biomolecule labeling, organelle imaging, cell tracking, tumor imaging and diagnosis, bacterial detection, *etc.*[10,11] Furthermore, with elegant molecular design, AIEgens with excellent photosensitization and controllable generation of various ROS types could be designed to fulfill different application requirements. Moreover, unlike conventional ACQ photosensitizers, these AIE photosensitizers with twisted structures show improved ROS production in the aggregate state, which further broadens their applications in PDT.[12]

This review summarizes the recent progress of AIE light-up probes in PDT. Firstly, precise molecular engineering strategies to develop efficient AIE photosensitizers are introduced, which is followed by the elaboration of the design concepts of AIE light-up probes. As the main part of this review, the PDT applications of AIE light-up probes are further discussed in detail from two aspects of photodynamic antitumor and antibacterial applications. These examples are categorized and discussed based on their different light-up mechanisms, including binding-mediated light-up, cleavage reaction-mediated light-up, bioorthogonal reaction-mediated light-up, external stimuli-mediated light-up, *etc.* Finally, a brief summary and further perspectives are discussed. AIEgens provide a path for developing light-up probes with high signal-to-noise ratios, high sensitivity, controllable photosensitization, *etc.* The reasonable design and development of AIE light-up probes shall greatly stimulate the development of PDT in disease treatment and practical applications.

2. Design of AIE light-up probes

2.1. Design of AIE photosensitizers

The theranostic effect of PDT is based on the photochemical reactions between excited photosensitizers and the surrounding oxygen or biological substrates. Such photosensitization process can be illustrated with a Jablonski diagram (Fig. 1a).[13] Upon photon absorption, photosensitizers will be excited from the ground state (S_0) to the singlet electronic state (S_n) and rapidly dissipate to the lowest excited singlet state (S_1). From S_1, photosensitizers could undergo a radiative decay process to S_0 to emit fluorescence or undergo nonradiative decay to S_0 to dissipate energy *via* molecular motion or collision with solvents. Alternatively, photosensitizers could also undergo the ISC process to the lowest triplet excited state (T_1) and further to S_0.[14] As the $S_1 \rightarrow T_1$ and $T_1 \rightarrow S_0$ processes involve electron spin orbital changes and are forbidden processes, photosensitizers at the T_1 state have a relatively long lifetime which provides sufficient time for photosensitizers to interact with the surrounding oxygen or biological substrates to generate ROS.[15,16] As the energy absorbed by a material is fixed, these three energy dissipation pathways are usually competitive;[17,18] therefore, AIEgens are advantageous in developing photosensitizers because they show largely inhibited nonradiative processes at the aggregate state, which could largely promote both the fluorescence and ISC that are beneficial for image-guided PDT.

To develop AIE photosensitizers with improved photosensitization ability, it is necessary to promote ISC processes. While introducing heavy atoms to enhance spin orbital coupling (SOC) could improve the ISC process,[19,20] the dark toxicity of heavy atoms limits their practical applications. In this regard, the most adapted approach is to reduce the S_1–T_1 energy gap (ΔE_{ST}) to boost ISC processes. Such approach is mainly achieved *via* a donor–acceptor (D–A) molecular engineering strategy to separate the HOMO–LUMO distribution, as it could reduce the repulsion between valence electrons with opposite spins in the S_1 state to achieve a smaller ΔE_{ST}.[12,21] A series of AIEgens with different degrees of HOMO–LUMO separation based on the tetraphenylethylene (**TPE**) skeleton were designed by Liu's group to demonstrate the feasibility of this strategy (Fig. 1a).[22,23] For example, methoxy and dicyanovinyl groups were introduced into the **TPE** skeleton as an electron donor and acceptor to form **TPDC**. **TPDC** showed a smaller ΔE_{ST} value of 0.48 eV as compared to that of **TPE** (1.27 eV), which endowed **TPDC** with the photosensitization ability but not **TPE**. When a benzene ring was further introduced to increase the dihedral angle between **TPE** and the electron accepter, the more separated HOMO–LUMO distribution was observed for **TPPDC**, and the ΔE_{ST} value was reduced to 0.35 eV. Moreover, such ΔE_{ST} value could be further decreased to 0.27 eV for **PPDC** when the benzene ring was used as the π-bridge to prolongate the conjugation length between the donor and the acceptor. With the decreased ΔE_{ST} values, the singlet oxygen ($^1O_2$) quantum yields of **TPDC**, **TPPDC**, and **PPDC** have been significantly improved, from 28% to 32% to 89%, using rose bengal (RB) as a standard and 9,10-anthracenediyl-bis(methylene)-dimalonic acid (ABDA) as an indicator.

To further bathochromically shift the absorption/emission band for improved penetration depth, a benzothiadiazole (BT) unit as the auxiliary acceptor and a phenyl ring as the π-bridge were introduced into **TPPDC** to afford D–A′–π–A type **TPEBTDC**. As compared to **TPPDC**, **TPEBTDC** exhibits larger dihedral angles, longer conjugation length, and a smaller ΔE_{ST} value (0.33 eV). As a result, **TPEBTDC** nanoparticles demonstrated a red-shifted absorption band and a 10.8-fold enhancement of $^1O_2$ production efficiency as compared to **TPPDC** nanoparticles. In addition, when the strong electron withdrawing group tetracyanoanthra-*p*-quinodimethane (TCAQ) was introduced into the **TPE** skeleton to further red-shift the emission wavelength, the electron cloud of the LUMO was located mainly on the TCAQ acceptor, leading to further HOMO–LUMO separation with an extremely small ΔE_{ST} value of 0.067 eV.[24] The resultant **TPETCAQ** showed NIR emission centered at 820 nm, making it the ideal candidate for image-guided *in vivo* PDT.

Besides the selection of different D–A pairs, increasing D or A numbers and further polymerizing into conjugated polymers represents another promising strategy to design AIE photosensitizers (Fig. 1b).[25,26] Liu's group demonstrated such polymerization-enhanced photosensitization in 2018.[25] They

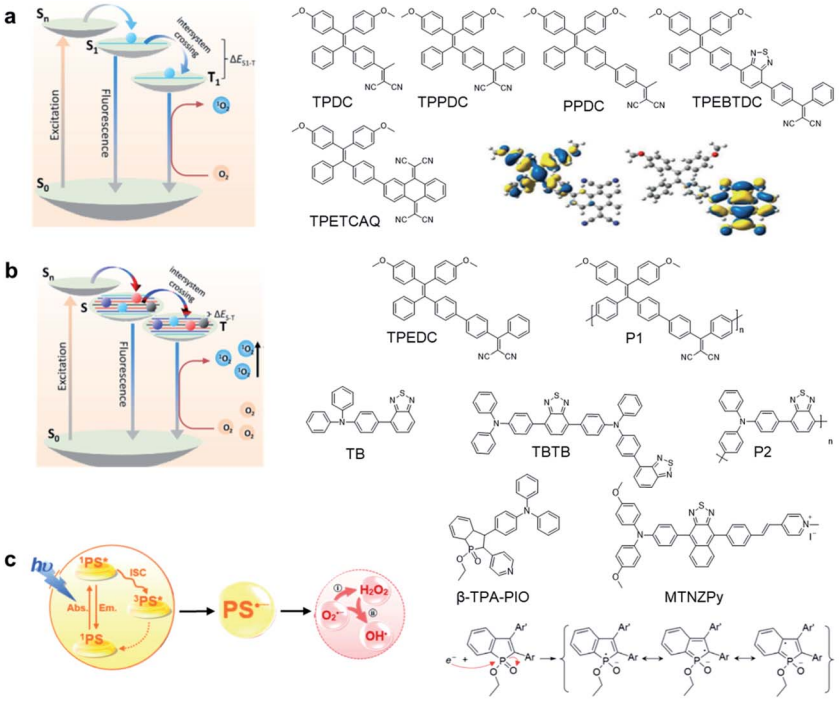

Fig. 1 Design principles and examples of AIE photosensitizers by (a) donor–acceptor engineering; (b) polymerization; (c) developing type-I photosensitizers. Reproduced from ref. 25 and 30 with permission. Copyright 2018 Elsevier, and 2020 The Royal Society of Chemistry.

selected **TPEDC** as the repeat units, and the corresponding conjugated polymers **P1** ($M_w = 17\ 000\ g\ mol^{-1}$) showed a 5-fold enhancement of $^1O_2$ generation as compared to **TPEDC**. In addition, **P1** also exhibited a red-shifted absorption band and enhanced absorption coefficients due to increased conjugation length, beneficial for *in vivo* applications. In a separate study, Tang and coworkers also demonstrated the feasibility of such polymerization-enhanced photosensitization strategy.[26] Triphenylamine (TPA, denoted as T) and BT (denoted as B) as an electron donor and acceptor were used to construct AIE photosensitizers with different repeat units (Fig. 1b). Along with the increased conjugation, the **TB**, **TBTB**, and **P2** (with 5 **TB** repeat units) nanoparticles showed increasing ROS production, with $^1O_2$ quantum yields of 3.8%, 8.9% and 14%, respectively, independent of nanoparticle sizes and shapes. Furthermore, decreased fluorescence quantum yields were observed with increased repeat units, and such inverse correlation suggests that polymerization is an effective approach to improve ISC processes. Both studies have applied theoretical calculation with time-dependent density functional theory (TD-DFT) to help gain insight into such strategy. It revealed that with increased conjugation length or repeat units, the multiple energy levels broaden the energy bands of these polymers, which lowers the upper excited states and raises the lower excited states. Further polymerization could lead to the fusion of S_n and T_n, making it possible for multiple ISC processes to occur, facilitating better photosensitization performance.

While the above D–A molecular engineering and polymerization strategies are aimed at boosting ISC processes to promote ROS production, they pay less attention to the types of generated ROS and these photosensitizers mainly generate $^1O_2$ (type-II). Different from type-II photosensitizers, type-I photosensitizers involve electron transfer between triplet photosensitizers and biological substrates to generate toxic free radical species such as superoxide anions ($O_2^{-\bullet}$), hydroxyl radicals (HO·), *etc.*[27] As oxygen is recycled in the superoxide dismutase (SOD)-mediated disproportionation reactions, type-I photosensitizers are less dependent on oxygen and more suitable for PDT under a hypoxic microenvironment.[28,29] Very recently, Zhuang *et al.* reported a type-I AIE photosensitizer based on phosphindole oxide (PIO).[30] The photosensitizer (**β-TPA-PIO**) is composed of a PIO core, triphenylamine (TPA) and pyridine (Py) (Fig. 1c). Indeed, the PIO core has three main functions: (1) it acts as an electron acceptor in the D–A structure; (2) its high electron affinity helps attract and stabilize external electrons; and (3) the heavy atom effect accelerates the ISC processes. Upon excitation, the phosphorous phosphine center attracts external electrons and destroys the phosphine oxygen bond to form a radical anion, which further transfers the electron to the surrounding substrate to form a radical ROS. Moreover, the addition of bovine serum albumin (BSA) could further promote free radical generation as BSA serves as an external electron donor. Another example of type-I AIE photosensitizers is **MTNZPy**, where methoxyl-substituted-TPA is connected to naphtha[2,3-*c*][1,2,5]thiadiazole (NZ) and serves as the electron donor, while the styrene pyridinium cation acts as the acceptor.[31] The free radical ROS generation is attributed to the cooperation of the intramolecular charge transfer (ICT) effect as well as the electron-rich anion–π^+ AIEgens, which promote the electron transfer process for free radical generation.

Table 1 Summary of AIE photosensitizers

Name	Chemical structure	Absorption (nm)	Emission (nm)	Quantum yield	Ref.
TPDC	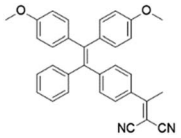	400 (DMSO)	600 (DMSO/Water = 1/99)	—	23
TPPDC	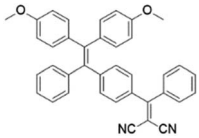	420 (DMSO/water = 1/99)	630 (DMSO/water mixtures)	21%	22
PPDC	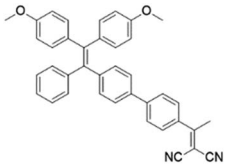	390 (DMSO)	600 (DMSO/water = 1/99)	—	23
TPEBTDC	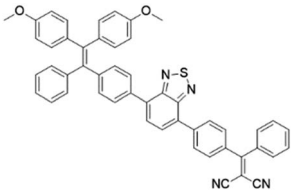	450 (DMSO/water = 1/99)	650 (DMSO/water mixtures)	10%	22
TPETCAQ	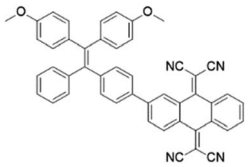	520 (THF)	820 (THF/water = 1/99)	—	24
TPETH	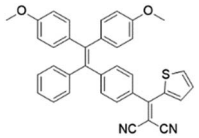	431 (DMSO/water = 1/99)	636 (DMSO/water mixtures)	17%	22
β-TPA-PIO	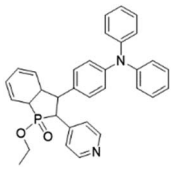	400 (DMSO)	614 (DMSO)	12.4% (DMSO)	30
MTNZPy	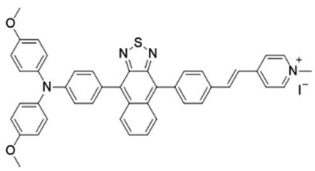	528 (DMSO)	686 (DMSO)	—	31
TPCI	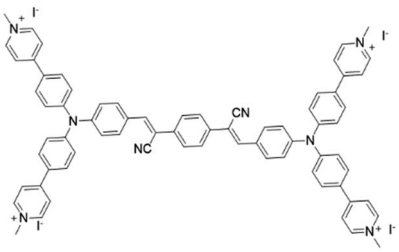	441	—	0.002 (water)	37

Table 1 (*Contd.*)

Name	Chemical structure	Absorption (nm)	Emission (nm)	Quantum yield	Ref.
TTVP	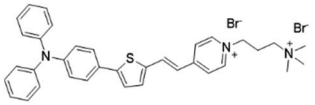	480 (water)	708 (aggregation state)	1.7% (aggregation state)	46
TPE-IQ-2O	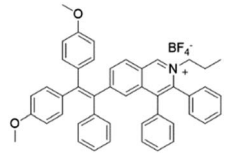	430 (DMSO)	620 (THF/hexane = 1/99)	13.1% (THF/hexane = 1/99)	50
IQ-TPA	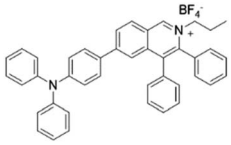	450 (DMSO)	622 (DMSO/water = 1/99)	—	51
TPE-DPA-TCyP	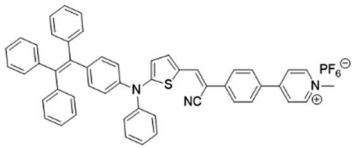	504 (DMSO)	697 (DMSO)	—	53
TFPy	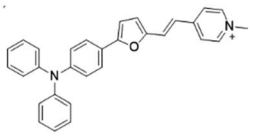	485 (DMSO)	684 (DMSO)	0.4% (DMSO)	54
TFVP	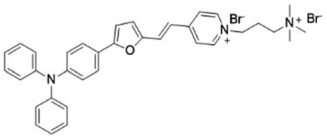	492 (water)	675 (water)	0.4% (water)	54
TPE-TFPy	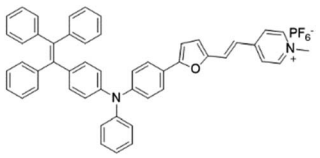	490 (DMSO)	672 (DMSO)	0.5% (DMSO)	54
TPy	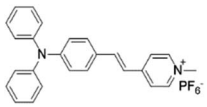	458 (DMSO)	618 (aggregation state)	4.7% (solid state)	75
TPPy	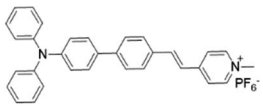	427 (DMSO)	645 (aggregation state)	7.6% (solid state)	75
TTPy	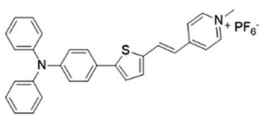	478 (DMSO)	665 (aggregation state)	9.6% (solid state)	75
MeOTTPy	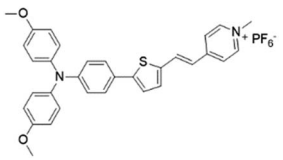	500 (DMSO)	664 (aggregation state)	2.9% (solid state)	75

Table 1 (*Contd.*)

Name	Chemical structure	Absorption (nm)	Emission (nm)	Quantum yield	Ref.
TPE-TTPy	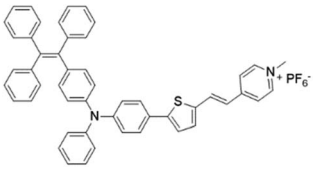	484 (DMSO)	665 (aggregation state)	4.9% (solid state)	75

With these strategies, various AIEgens with improved absorption, red-shifted emission, and enhanced ROS production have been developed, and Table 1 summarizes the photophysical properties of these AIE photosensitizers, which await further engineering for real practical applications.[32–35]

2.2. Design concepts of AIE light-up probes

2.2.1 Aggregation-induced light-up. Owing to the unique nature of AIEgens, a multitude of light-up probes have been developed in accordance with the RIM mechanism. These AIE light-up probes normally exhibit sufficient water solubility to diminish the fluorescence *via* active intramolecular motions, and they could be categorized into two groups based on the different approaches to induce RIM: binding-induced light-up and reaction-induced light-up. As shown in Fig. 2a, the binding-induced light-up probes mainly use binding ligands to physically attract the accumulation of multiple AIE probes at targets.[36] Binding to the target analyte results in the restriction of the AIEgen movement, which suppresses the nonradiative decay process and activates a radiative pathway to realize the fluorescence. This binding could be induced by specific targeting ligands, antibodies or peptides, or through non-covalent forces such as electrostatic interaction, hydrogen bond interaction, *etc.* **TPCI** is one of such AIE light-up probes for specific labelling of the cell nucleus.[37] The four peripheral pyridine salts of **TPCI** endow it with a strong binding affinity for DNA, allowing it to specifically target, accumulate and light up the cell nucleus.

Reaction-induced light-up probes are generally designed to form a strong luminescent product through a chemical reaction (Fig. 2b). There are generally two kinds of chemical reaction involved: removal of the water-soluble segments (such as enzyme digestion reaction), and covalent binding to target analytes (such as bioorthogonal reaction).[38,39] One example is **TPECM-2GFLGD$_3$-cRGD** reported by Yuan *et al.*[40] In this case, TPECM acts as an AIE photosensitizer with both imaging and therapeutic functions; GFLG is a responsive peptide of cathepsin B which is a lysosomal protease overexpressed in many types of tumor; D_3 is a hydrophilic group that endows the probe with water solubility; cRGD can selectively target $\alpha_v\beta_3$ integrin. Due to the connection of the hydrophilic peptides, the probe had almost no fluorescence in water. The GFLG peptide was specifically cleaved by cathepsin B, which led to the aggregation of TPECM molecules. Compared with interaction-based probes, reaction-based probes are more specific and more adaptable to complex microenvironments.

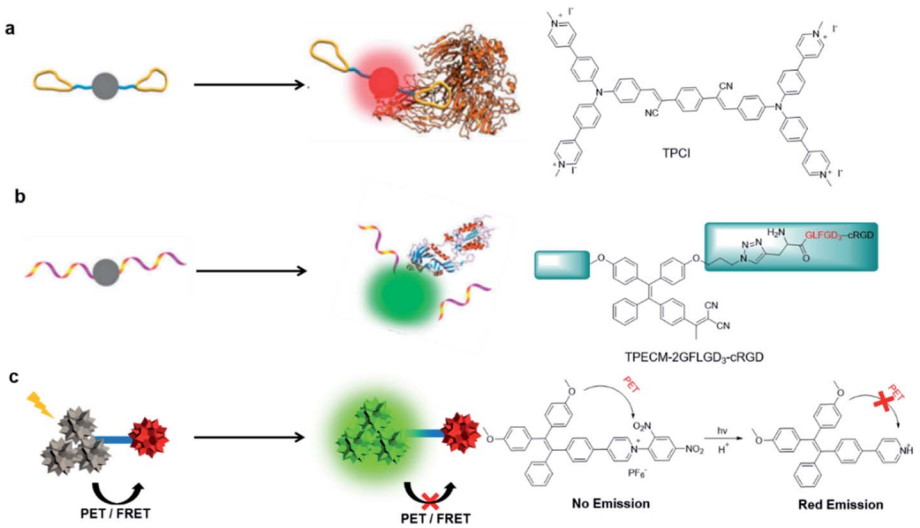

Fig. 2 Design concepts and examples of AIE light-up probes by (a) binding-induced light-up (b) reaction-induced light-up and (c) dequenching induced light-up. Reproduced from ref. 36 with permission. Copyright 2015 The Royal Society of Chemistry.

2.2.2 Dequenching induced light-up. In addition to the unique aggregation-induced light-up mechanism, these well-developed dequenching strategies for traditional probes are also applicable to AIEgens. To design light-up probes for conventional ACQ fluorophores, removing fluorescent quenchers is usually required as these water-soluble ACQ dyes are fluorescent in aqueous solution. However, aggregation is a natural process, and the high local density of ACQ probes at the targeting area could lead to compromised imaging and therapeutic performance even after the removal of quencher groups. In this regard, AIEgens with strong emission in aggregates represent an ideal candidate to design light-up probes through dequenching strategies. Fluorescence resonance energy transfer (FRET) and photoinduced electron transfer (PET) are the two main photophysical processes that are used to achieve fluorescence and ROS quenching. FRET is largely dependent on the emission and absorption spectrum overlap between the donor and acceptor as well as their distance.[41] Therefore, specific reactions that could break such spectrum overlaps or close distance could recover the emission and ROS production of the donor photosensitizers. Differently, PET is a photophysical process in which electrons are transferred from an electron donor to an electron accepter under the induction of light.[42] Since PET directly competes with other radiative and nonradiative deactivation processes in the excited state, it plays an extremely important role in quenching fluorescence.[43] Therefore, the interruption of the PET process under appropriate conditions can also realize the light-up of AIE probes. For example, Zhang's group reported one of this kind of AIE probe (Fig. 2c).[44] Due to the PET process from the **TPE** unit to the 1-(2,4-dinitrophenyl) pyridinium unit (electron accepter), the probe hardly emits fluorescence even in the aggregate state. The removal of 2,4-dinitrophenyl under light illumination breaks PET processes, resulting in strong green fluorescence emission. The protonation of pyridine under an acidic environment could further enhance the ICT process, leading to red-shift emission and activated PDT.

3. AIE light-up probes for antitumor applications

PDT as a noninvasive treatment has been actively used in clinical practice of skin cancer, bladder cancer and so forth. The development of light-up probes further helps to identify tumor tissues for more accurate light treatments. In this section, we elaborate on the recent development of AIE light-up probes for photodynamic antitumor applications.

3.1. Binding-mediated light-up probes

Abnormal expression of proteins (non-enzymatic) is often associated with many tumors, which makes them excellent targets for tumor monitoring and drug delivery. By attaching water-soluble tumor targeting ligands, AIE light-up probes have been widely used for PDT through a binding-mediated light-up approach. One of the early examples was reported in 2014 by Zhang's group where a light-up probe (**TPE-red-2AP2H**) was designed for specific photodynamic ablation of cancer cells with lysosomal transmembrane protein (LAPTM4B) over-expression.[45] **TPE-red-2AP2H** consists of two parts: red-emissive TPE-red with dual functions of imaging and therapy, and the specific peptide AP2H (IHGHHIISVG) with targeting ability toward the LAPTM4B protein. **TPE-red-2AP2H** showed specific red-fluorescence light-up on the cellular membrane of LAPTM4B-positive HepG2, HeLa and U2OS cancer cells, while it showed almost no fluorescence on HEK293 normal cells, demonstrating the high selectivity of the probe. In addition, TPE-Red is also an efficient photosensitizer which could generate $^1O_2$ under light irradiation to achieve targeted PDT under the guidance of high signal-to-noise ratio imaging.

Hydrophilic/hydrophobic and electrostatic interactions have also been used to construct light-up probes for image-guided PDT. Tang's group prepared the water-soluble NIR AIE probe **TTVP** for cell membrane targeted PDT.[46] The probe hardly emits in aqueous solution due to good water solubility originating from the positively charged quaternary ammonium and pyridinium ligands. These positively charged ligands further made it possible for **TTVP** to bind to negatively charged cell membranes especially cancer cell membranes which possess more negative surface charge. Upon interaction with the cell membrane, the hydrophilic part of the probe cannot quickly pass through the cell membrane due to the hydrophobic interior nature of the cell membrane, while the hydrophobic emitting segment is embedded into the hydrophobic region of the membrane bilayers. Such embedding limits the movement of AIE probe and realizes rapid no-wash imaging of the cell membrane within a few seconds (Fig. 3b). In addition, **TTVP** with a D–A structure has a small ΔE_{ST} (0.47 eV), making it an efficient NIR photosensitizer with a high $^1O_2$ quantum yield of 80.16%, which provides an opportunity for **TTVP** to kill cancer cells at very low concentrations (1 μM).

The precise subcellular localization and targeting in cells is indispensable for improving the theranostic effect. As the source of cell energy, mitochondrial dysfunctions may directly cause cell death, proliferation and metastasis. Therefore, the development of mitochondrial-targeted photosensitizers is of great significance for PDT.[47,48] Due to the high membrane potential of mitochondria, a series of positively charged (such as triphenylphosphine, pyridine salt, and quaternary ammonium salt) probes were designed to specifically target mitochondria.[49] For example, **TPE-IQ-2O** with a pyridine moiety can specifically target the mitochondria of cancer cells but not normal cells and cause specific ablation of cancer cells under white light irradiation.[50] This is due to the difference in mitochondrial membrane potential between cancer cells and normal cells. To solve the short excitation wavelength issues, **IQ-TPA** with two-photon excitation was developed with deep penetration depth and precise spatial control (Fig. 3c).[51] **IQ-TPA** showed a large two-photon cross section of 213 GM and excellent photosensitization under two-photon excitation, which made it suitable for two-photon image-guided PDT. Under 900 nm two-photon laser scanning, **IQ-TPA** showed great potential in photodynamic ablation of cancer cells with very high spatial control. Besides improving the excitation

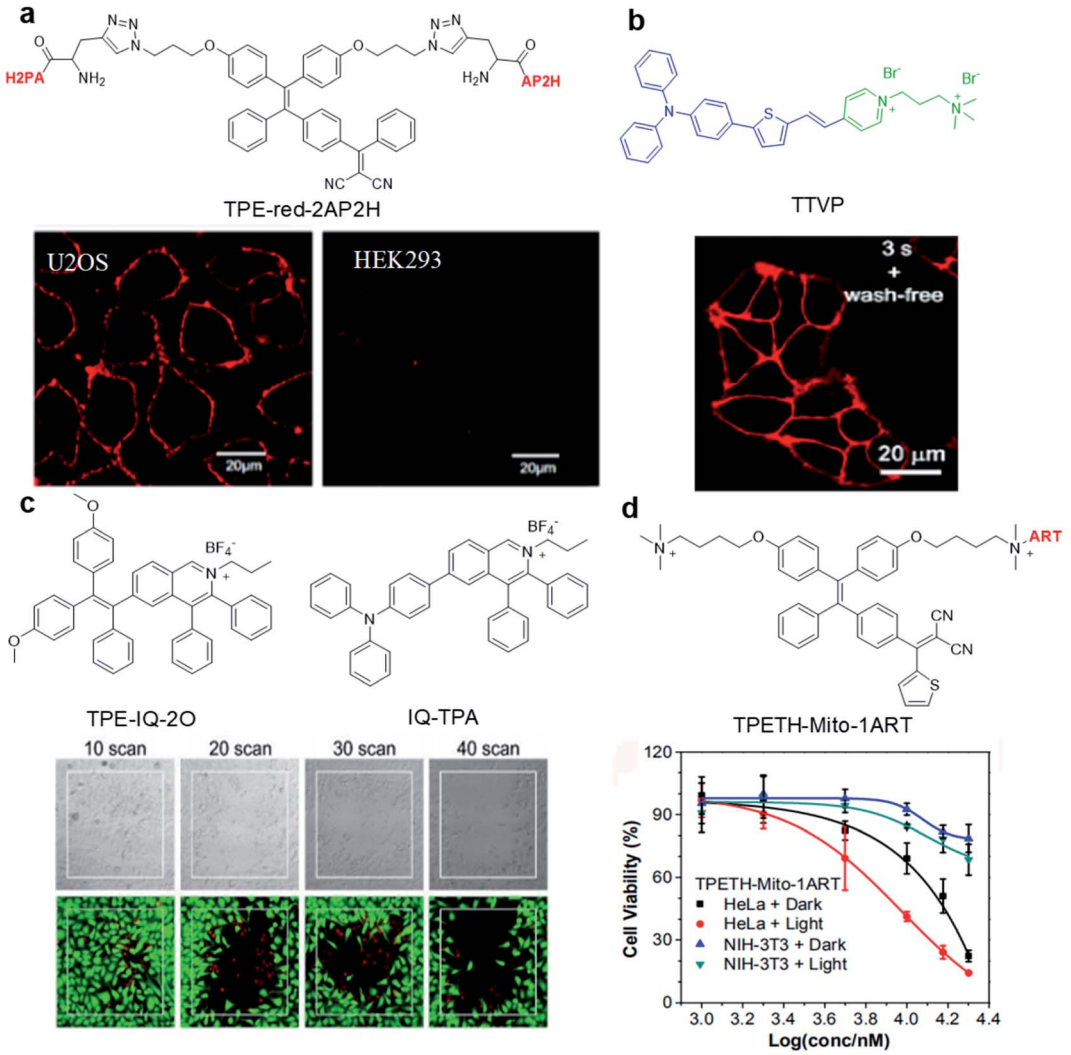

Fig. 3 (a) Chemical structure of **TPE-red-2AP2H**; CLSM images of U2OS and HEK293 cells after incubation with **TPE-red-2AP2H** (10 μM) in acidic environments. Reproduced from ref. 45 with permission. Copyright 2014 American Chemical Society. (b) Chemical structure of **TTVP**; CLSM image of living HeLa cells after incubation with **TTVP** (500 nM). Reproduced from ref. 46 with permission. Copyright 2018 The Royal Society of Chemistry. (c) Chemical structures of **TPE-IQ-2O** and **IQ-TPA**; live (green, FDA)/dead (red, PI) staining of **IQ-TPA** treated HeLa cells under two-photon scanning. Reproduced from ref. 51 with permission. Copyright 2018 The Royal Society of Chemistry. (d) Chemical structure of **TPETH-Mito-1ART**; viabilities of HeLa and NIH-3T3 cells after treatment with **TPETH-Mito-1ART** for 2.5 h with or without white light treatment (60 mW cm^{-2}, 10 min). Reproduced from ref. 52 with permission. Copyright 2018 American Chemical Society.

wavelength, combining PDT with other therapeutic modalities has also attracted great research interest. In 2018, Feng *et al.* reported a mitochondrial-targeted light-up probe (**TPETH-Mito-1ART**) to achieve the co-delivery of artemisinin and AIE photosensitizers to cancer cell mitochondria for combination therapy (Fig. 3d).[52] The probe basically has no emission in aqueous solution, but it can selectively accumulate in the mitochondria of tumor cells instead of normal cells to achieve fluorescence turn-on. As mitochondria is also the main target of artemisinin, such co-delivery showed synergistic killing effects, which rapidly depolarized the mitochondrial membrane and reduced cancer cell migration, demonstrating the great potential of AIE conjugates in combination therapy.

Mitochondria-anchoring AIE photosensitizers could also generate mitochondrial oxidative stress, which can be used to induce immunogenic cell death (ICD) for antitumor treatment. ICD is a type of apoptotic cell demise that could reverse the poor immunogenicity suffered by many cancers, the induction of ICD could promote dendritic cell maturation and initiate adaptive antitumor immunity. The use of AIE photosensitizers as ICD inducers was firstly reported by Ding's group in 2019 with **TPE-DPA-TCyP** as the example (Fig. 4).[53] With a D–π–A structure, rich rotary units, and a pyridinium moiety, **TPE-DPA-TCyP** showed weak emission in aqueous solution, but bright FR/NIR fluorescence in aggregates such as inside lipid vesicles or in cancer cell mitochondria. Moreover, the twisted structure and large HOMO–LUMO separation helped to reduce the ΔE_{ST} value to 0.23 eV, endowing **TPE-DPA-TCyP** with excellent ROS generation ability. Benefiting from the pyridinium moiety, **TPE-DPA-TCyP** was mainly distributed in the mitochondria of the 4T1 cancer cell to

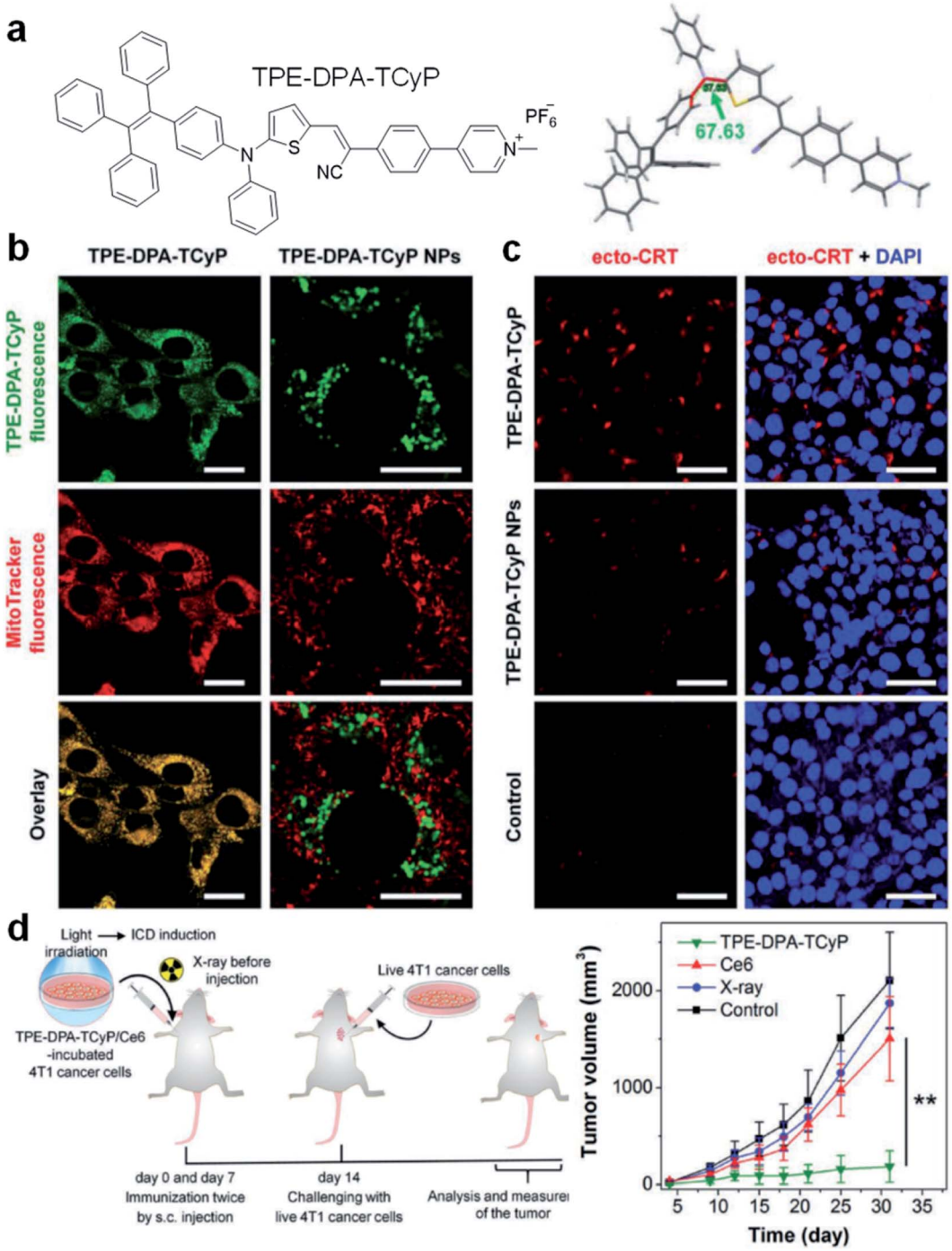

Fig. 4 (a) Chemical structure of **TPE-DPA-TCyP**. (b) CLSM images of 4T1 cancer cells treated with **TPE-DPA-TCyP** or **TPE-DPA-TCyP** nanoparticles (NPs), which were co-stained with commercial MitoTracker Deep Red FM. (c) CLSM images displaying the ecto-CRT expression (red fluorescence) of 4T1 cells after incubation with **TPE-DPA-TCyP** (0.2 μM) or **TPE-DPA-TCyP** NPs (0.72 μM), respectively, at 37 °C for 90 min and subsequent light irradiation (10 mW cm^{-2}) for 1 min. The cell nuclei were stained with 4′,6-diamidino-2-phenylindole (DAPI: blue fluorescence). (d) Schematic illustration of using a prophylactic tumor vaccination model to evaluate the *in vivo* ICD immunogenicity of different ICD inducers, and the plot of tumor volume growth in different groups indicated *versus* the time post live 4T1 cancer cell inoculation. Reproduced from ref. 53 with permission. Copyright 2019 Wiley-VCH.

light up its fluorescence, with an overlap coefficient of 0.839 with MitoTracker Deep Red FM (Fig. 4b). The directly generated ROS at the cancer cell mitochondrion site could massively induce ICD *via* up-regulation of PERK-mediated eIF2α phosphorylation, as indicated by the translocation of surface-exposed calreticulin (ecto-CRT) (Fig. 4c). To study the role of focused mitochondrial oxidative stress in ICD induction, **TPE-DPA-TCyP** nanoparticles with alerted intracellular distribution were used as a control.

TPE-DPA-TCyP nanoparticles cannot target mitochondria, and their ability to induce ecto-CRT is far less than that of pure **TPE-DPA-TCyP**, proving that ROS-induced mitochondrial stress is an extremely effective strategy to amplify ICD. Moreover, **TPE-DPA-TcyP** also showed much higher ecto-CRT induction as compared to other ICD inducers, such as secreted ATP, heat shock protein 70 (HSP70), chlorin **Ce6** photosensitizer, *etc.*, demonstrating the superior performance of mitochondria-anchoring AIE photosensitizers in boosting ICD. Subsequently, a prophylactic tumor vaccination model was established to evaluate the *in vivo* ICD immunogenicity of **TPE-DPA-TCyP** (Fig. 4d). The **TPE-DPA-TCyP** group showed much more efficient tumor growth suppression than X-ray and **Ce6** groups. Therefore, AIE photosensitizers with mitochondria-anchoring ability, 3D twisted structure, and abundant ROS generation in aggregates demonstrate a desirable platform for developing advanced ICD inducers.

In addition to combination therapy, multi-organelle targeting and multi-source PDT have also been found to be effective ways to improve the therapeutic effect. In 2020, Xu *et al.* synthesized three AIEgens sharing the same skeleton but with different moieties to target mitochondria (**TFPy**), cell membranes (**TFVP**) and lysosomes (**TPE-TFPy**) concurrently for multi-organelle targeted PDT (Fig. 5).[54] The co-localization test verified the high organelle specificity of these three AIEgens. The 4T1 cancer cell line was used as an example to evaluate the PDT effects of the "individual AIEgen" group and the "three-in-one" group (with 1/3 concentration of each AIEgen to ensure the same overall concentration). Although the "three-in-one" group showed lower ROS generation as compared to **TPE-TFPy** under light irradiation, it caused more cell death where the "three-in-one" group can eliminate over 90% cancer cells at 5 μM while the value is only around 40% for the "individual AIEgen" group. Further *in vivo* animal experiments also revealed better inhibition of tumor growth for the "three-in-one" group, proving that multi-organelle targeted PDTs exhibited a synergistic effect of "1 + 1 + 1 > 3".

3.2. Cleavage reaction-mediated light-up probes

As mentioned earlier, cleavage reaction-mediated light-up probes generally consist of a cleavable quencher and an AIE photosensitizer. The quenchers could be cleaved by a specific tumor microenvironment such as overexpressed enzymes, GSH, and acidic pH, which leads to the recovery of the fluorescence and photosensitization of the probe for activated PDT.[55–57] In 2018, Ding's group reported an activatable probe, **TPE-Py-FpYGpYGpY**, using the dephosphorylation reaction of the overexpressed alkaline phosphatase (ALP) in tumors (Fig. 6a).[58] The probe is a combination of TPE-Py as the AIE photosensitizer and a short peptide modified with three tyrosine phosphates as the reaction site. Benefiting from tyrosine phosphates, the AIE probe showed very weak fluorescence and low ROS generation ability. After ALP dephosphorylation, the water solubility of the probe decreases and it self-assembles into nanoaggregates, which activate its fluorescence and photosensitization for image-guided tumor cell ablation. The probe showed very high specificity toward ALP over other enzymes, and the presence of ALP inhibitor sodium orthovanadate (Na_3VO_4) could largely inhibit its fluorescence and ROS activation, further proving that such activation is specially derived from ALP dephosphorylation (Fig. 6b). As ALP is overexpressed on the surface of many cancer cells such as Saos-2 cancer cells, **TPE-Py-FpYGpYGpY** showed promising capability of differentiating these cancer cells from normal ones, and especially suppressing ALP-overexpressed cancer cells under photodynamic treatment (Fig. 6c).

As an important antioxidant in the body, glutathione (GSH) is overexpressed in a variety of tumor cells,[59] which has also been used as a trigger to turn on the theranostic effects of AIE probes. In 2017, Liu's group reported a GSH-mediated AIE light-up probe for combined photodynamic and chemotherapeutic treatment (Fig. 7a). The probe **TPEPY-S-MMC** is composed of an AIE photosensitizer, **TPEPY**, and a chemical prodrug, mitomycin C (**MMC**), linked through a GSH-cleavable S–S bond.[60] **MMC** chemotherapeutics can be used as fluorescence quenchers and $^1O_2$ quenchers through the mechanism of PET. After being internalized by the cancer cell, the disulfide bond is cleavage by GSH, and **TPEPY** and **MMC** are activated at the same time for combined treatment. The restored fluorescence can report the activation of photosensitizer and **MMC** in real time and guide PDT. Both *in vitro* and *in vivo* experiments

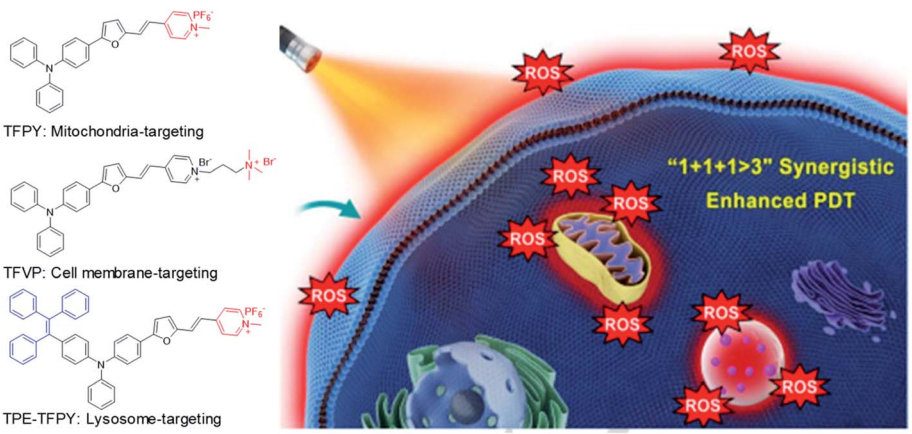

Fig. 5 Chemical structures of three AIEgens: TFPY, TFVP, and TPE-TFPY; schematic illustration of using three AIEgens for achieving "1 + 1 + 1 > 3" synergistic enhanced photodynamic therapy. Reproduced from ref. 54 with permission. Copyright 2020 Wiley-VCH.

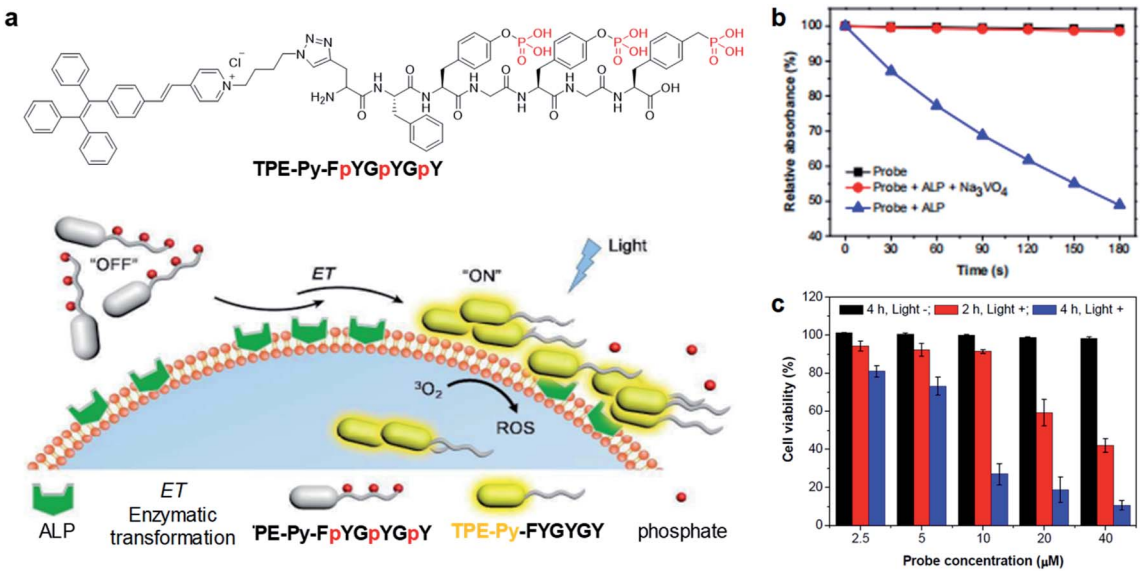

Fig. 6 (a) Schematic illustration of TPE-Py-FpYGpYGpY activation by ALP. (b) ABDA decomposition by different samples under light irradiation. (c) Cell viabilities of TPE-Py-FpYGpYGpY treated Saos-2 cancer cells, followed by white light (0.25 W cm^{-2}, 4 min) (referred to as "Light +") or dark treatment (referred to as "Light −"). Reproduced from ref. 58 with permission. Copyright 2018 The Royal Society of Chemistry.

revealed that the probe shows high selectivity for GSH to specifically light-up tumor tissues (Fig. 7b and c). GSH non-cleavable probe **TPEPY-C-MMC** was also used as a control to study its activation. Under light irradiation, **TPEPY-C-MMC**, **TPEPY-S-MMC**, or **TPEPY-C-MMC** + GSH cannot cause ABDA decomposition, and only the **TPEPY-S-MMC** + GSH group showed obvious ROS generation, indicating the specific ROS activation of **TPEPY-S-MMC** by GSH which helps to reduce off-target phototoxicity (Fig. 7d). **TPEPY-S-MMC** showed a much lower half-maximal inhibitory concentration (IC_{50}) on 4T1 cells

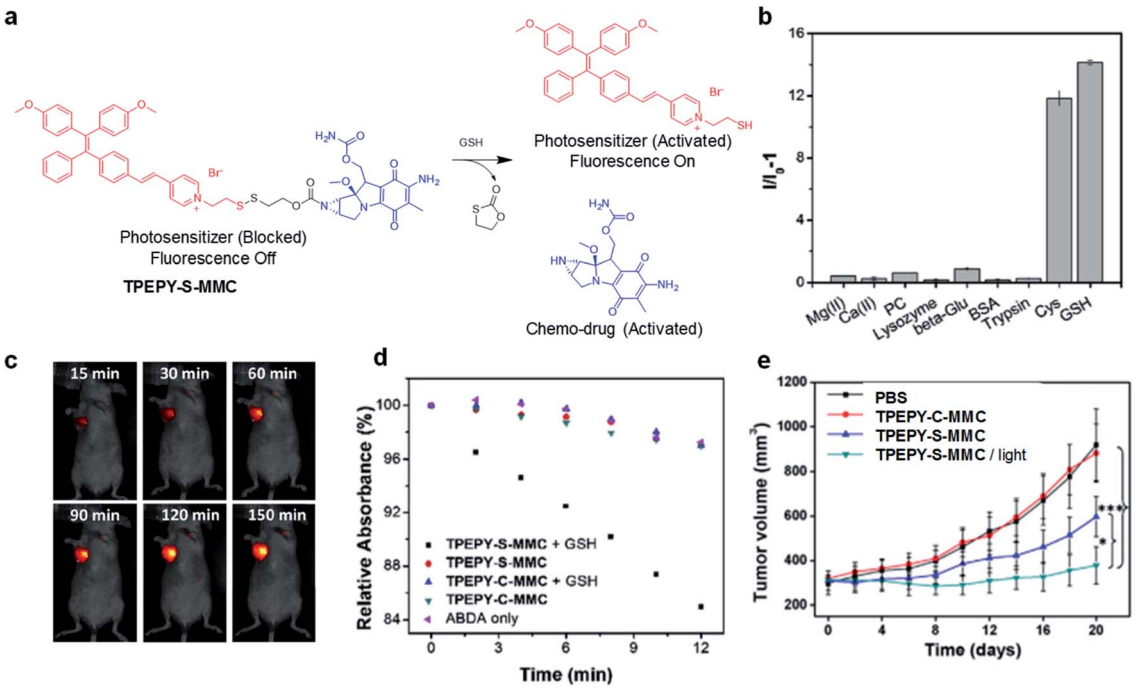

Fig. 7 (a) Traceable activation of dual-prodrug TPEPY-S-MMC by GSH. (b) Light-up of TPEPY-S-MMC upon treatment with different analytes; I_0 and I are fluorescence intensities of TPEPY at 660 nm before and after analyte treatment. (c) *In vivo* fluorescence imaging of 4T1 bearing mice after intratumoral administration of TPEPY-S-MMC. (d) ROS generation of TPEPY-S-MMC and TPEPY-C-MMC before and after GSH treatment as indicated by ABDA absorbance changes. (e) Tumor volume measurement after intratumoral administration with PBS, TPEPY-C-MMC and TPEPY-S-MMC without or with white light irradiation (0.10 W cm^{-2}, 3 min). Reproduced from ref. 60 with permission. Copyright 2017 Elsevier.

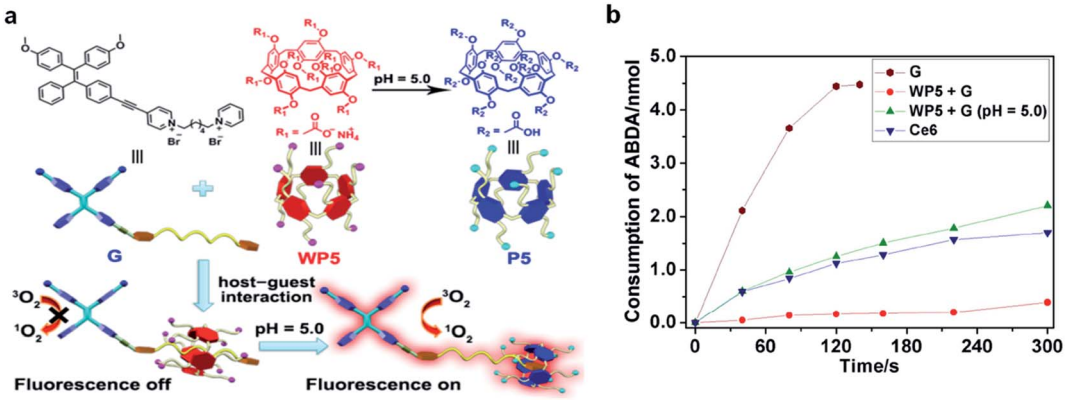

Fig. 8 (a) Schematic illustration of activation of **G** under an acidic environment. (b) Consumption of ABDA (5.0 nmol) in the presence of **G** (30 μM), **Ce6** (30 μM), and **WP5** + **G** (30 μM each) at pH = 5.0 under light irradiation. Reproduced from ref. 61 with permission. Copyright 2020 Wiley-VCH.

(3.7 μM) as compared to **TPEPY** and **MMC** (8.3 μM and 20.4 μM, respectively), showing the synergistic therapeutic effects. Furthermore, a tumor growth inhibition experiment in a tumor-bearing mouse model also revealed a much slower tumor growth for the **TPEPY-S-MMC**/light group, proving that the combination of PDT and chemotherapy has a better therapeutic effect (Fig. 7e). Such fluorescence/ROS/chemotherapy activation only occurred at specific tumor sites, which helped to minimize the background signal interfaces from other healthy issues and also largely reduced the toxic side effects to these normal organs.

Very recently, a host–guest complexation system was reported by Huang's group for fluorescence and ROS activation in response to the acidic tumor environment.[61] An AIE photosensitizer (**G**) was selected as the guest molecule, and a water soluble pillar[5]arene (**WP5**) was used as the host (Fig. 8a). In a neutral environment, the long hexyl chain on **G** provides the binding sites for host–guest complexation, which penetrated into the cavity of **WP5** to form a pseudorotaxane structure. The fluorescence and photosensitization properties of **G** are quenched by **WP5** *via* PET. In an acidic environment, **WP5** is protonated to neutral **P5**, which slipped out of the alkyl chain of

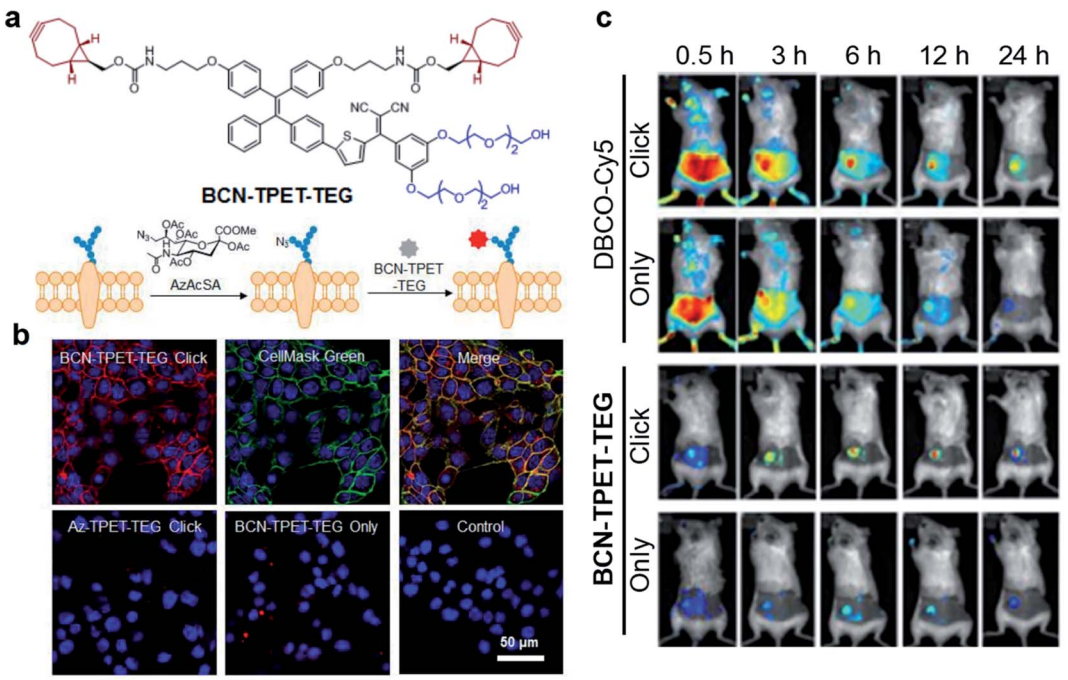

Fig. 9 (a) Chemical structure of **BCN-TPET-TEG** and schematic illustration of bio-orthogonal labeling-mediated light-up of **BCN-TPET-TEG** on the cell membrane. (b) Confocal images of 4T1 cells after **BCN-TPET-TEG** (5 μg mL^{-1}) bio-orthogonal labeling; CellMask Green is used for the colocalization test. (c) Fluorescence images of DBCO-Cy5 or **BCN-TPET-TEG** treated 4T1-bearing mice with/without AzAcSA pretreatment. Reproduced from ref. 65 with permission. Copyright 2018 Wiley-VCH.

G and moved to the terminal pyridine unit. Such shuttle movement interrupted the PET process and led to the coprecipitation of **P5** and **G**, resulting in the recovery of fluorescence and ROS generation of **G**. With a low ΔE_{ST} of 0.2 eV, **G** represented a better photosensitizer over commercially used **Ce6**; however it also demonstrated obvious dark cytotoxicity that is not suitable for PDT. Intriguingly, such a host–guest complexation system could not only suppress its ROS generation under light but also inhibit its dark cytotoxicity, which potentially overcame the "always-on" phenomenon and reduced the damage to normal tissues (Fig. 8b).

3.3. Bio-orthogonal reaction mediated light-up probes

Bioorthogonal reaction refers to these chemical reactions that could proceed efficiently in a living system with minimal effect on biology, which demonstrates promising potential in bioimaging and drug delivery technology.[62–64] The combination of bioorthogonal reaction with AIE could utilize the RIM mechanism to provide imaging with high specificity and signal-to-noise ratio. Recently, Liu's group reported a bioorthogonal reaction-mediated light-up AIE probe with very high tumor specificity for image-guided PDT.[65] The probe **BCN-TPET-TEG** was designed by connecting hydrophilic triethylene glycol (TEG) and copper-free clickable bicycle[6.1.0]nonyne (BCN) to the AIE core (TPET) (Fig. 9a). The probe hardly emitted fluorescence in aqueous solution due to its excellent water solubility benefiting from TEG groups, which also reduced the nonspecific interactions in biological systems. A metabolic precursor, AzAcSA, was firstly applied to cancer cells to introduce azide groups on cancer cell surfaces through sugar metabolism. When such cancer cells were further treated with **BCN-TPET-TEG**, these probes could be covalently bound to the cell surface through a copper-free click bioorthogonal reaction. Such bioorthogonal reaction could inhibit the intramolecular motion of TPET,

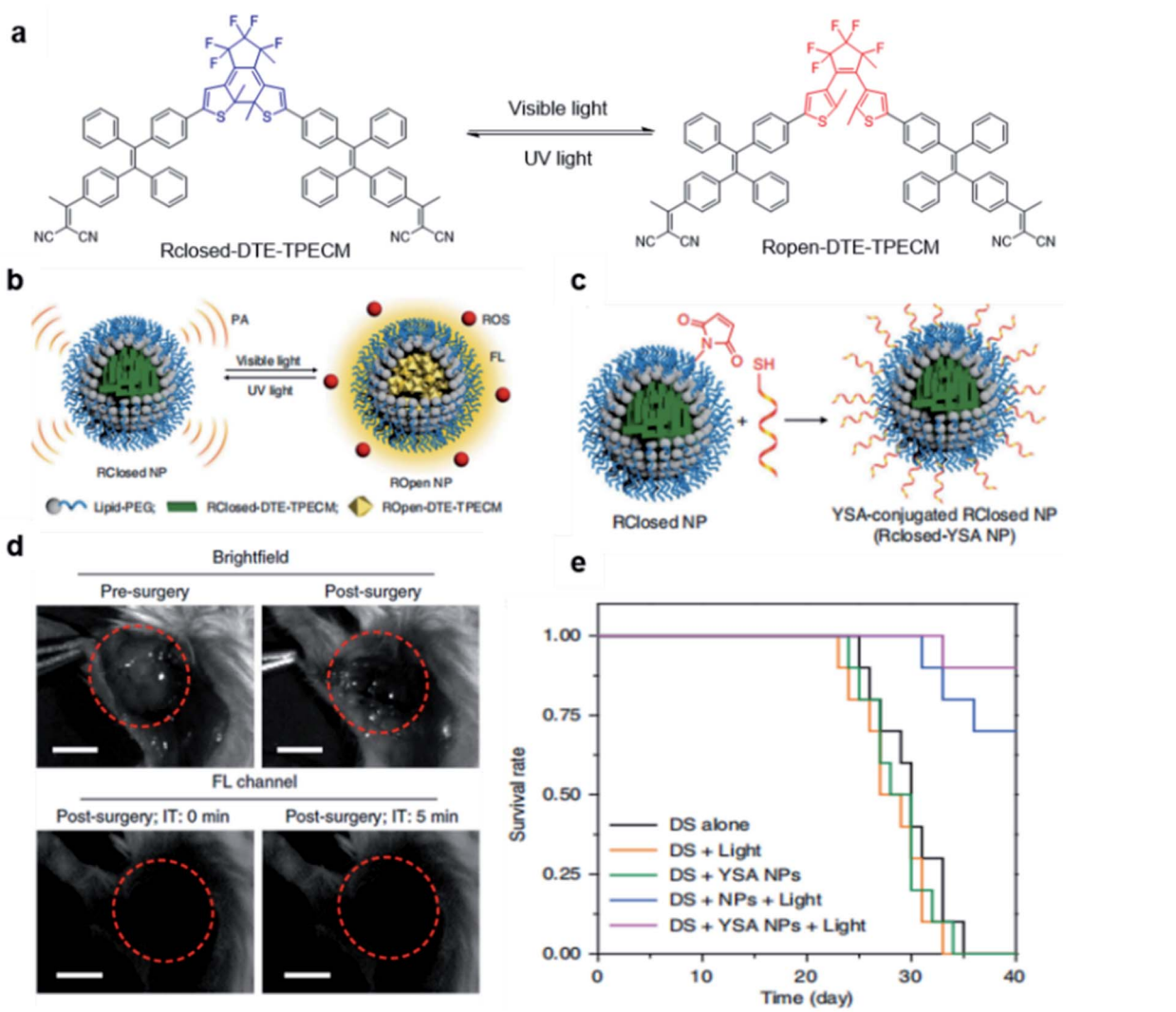

Fig. 10 (a) Chemical structures of photo-controllable **DTE-TPECM** molecules. (b) Schematic illustration of RClosed and ROpen nanoparticles. (c) Schematic illustration of the preparation of RClosed-YSA nanoparticles. (d) Representative images of tumor-bearing mice before and after surgery with or without fluorescence guidance; scale bars, 3 mm. (e) Mouse survival curves for different groups. Reproduced from ref. 66 with permission. Copyright 2018 Nature Publishing Group.

resulting in a strong red fluorescence turn-on (Fig. 9b). In contrast, very weak fluorescence can be observed for cancer cells only treated with **BCN-TPET-TEG**, indicating the promise of bioorthogonal reaction to turn on the emission of AIE probes. Moreover, the *in vivo* tumor imaging with intravenous injection further demonstrated the great advantage of AIE probes in bioorthogonal imaging as compared to conventional "always-on" fluorophores, where AIE probes showed rapid fluorescence turn-on only at tumor sites with no detectable signal from the rest of the mouse body. The bioorthogonal reaction also helped to reduce tumor clearance as the probes are covalently linked to cancer cells, which allows for better tumor imaging and therapeutic outcomes (Fig. 9c). As a highly effective photosensitizer with 59.1% $^1O_2$ generation efficiency, **BCN-TPET-TEG** demonstrated its powerful ability in photodynamic inhibition of tumor growth.

3.4. External stimuli-mediated light-up probes

Besides utilizing the specific binding or reaction to light up the fluorescence of AIE probes, external stimuli have also been reported to activate fluorescence and PDT effects of AIEgens for tumor treatment. Tang and Ding's groups developed a transformable molecule whose energy deactivation pathways can be

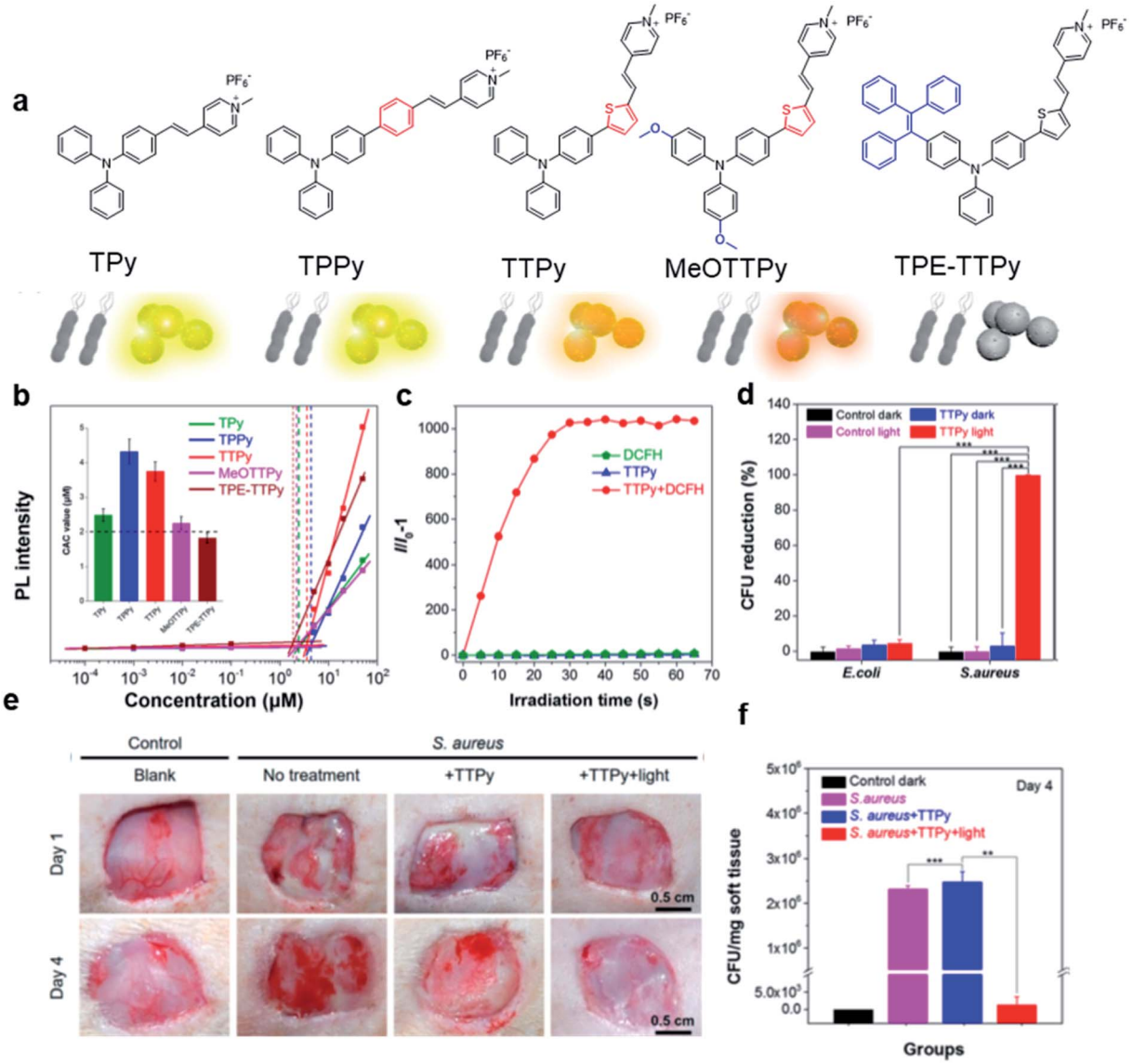

Fig. 11 (a) Molecular structures of **TPy**, **TPPy**, **TTPy**, **MeOTTPy**, and **TPE-TTPy**. (b) Plots of fluorescence intensities of AIEgens *versus* dye concentrations in PBS solution. Inset: Corresponding statistical histogram of the critical aggregation concentrations (CAC) of AIEgens. (c) ROS generation of **TTPy** (1 μM) upon white light irradiation using dichlorofluorescin (DCFH) as an indicator, where I_0 and I are fluorescence intensities of DCFH before and after light irradiation. (d) Colony-forming unit (CFU) reduction of *E. coli* and *S. aureus* with/without **TTPy** (2 μM) and white light (60 mW cm^{-2}) treatment. (e) Photographs of *S. aureus*-infected wounds after treatment with **TTPy** with/without white light irradiation (60 mW cm^{-2}) on day 1 and day 4 post-infection. (f) Statistical histogram of bacterial colonies on the agar plates originating from the infected sites on rats with different treatments. Reproduced from ref. 75 with permission. Copyright 2019 American Chemical Society.

switched by external light irradiation for image-guided tumor surgery and post-surgery PDT.[66] The molecule (**DTE-TPECM**) consists of two TPECM units and a dithiophene ethylene (DTE) core (Fig. 10a). External UV/visible light irradiation could realize repeatable conversion between the open loop and closed loop formats of the molecule. In the relatively flat **RClosed-DTE-TPECM** molecule, energy is mainly lost through thermal deactivation, making **RClosed-DTE-TPECM** ideal for photoacoustic imaging. In contrast, the relatively twisted 3D **ROpen-DTE-TPECM** molecular structure inhibits π–π stacking and the thermal deactivation pathway, thereby activating fluorescence emission and ROS production. **RClosed-DTE-TPECM** is further encapsulated by DSPE-PEG_{2000} and functionalized with the targeting ligand YSA (CYSAYPDSVPMMS) to afford RClosed-YSA nanoparticles for *in vivo* targeting of EphA2 overexpressed cancer cells (Fig. 10b and c). Animal experiments revealed the feasibility of such function-switchable nanoparticles for improving cancer surgery outcomes. RClosedYSA nanoparticles showed excellent photoacoustic signals with an improved signal-to-noise ratio, which can be used for preoperatively locating and identifying tumors for tumor removal surgery. Visible light irradiation activates a fluorescence signal and ROS for intraoperative surgery guidance and post-surgery treatment. Fluorescence imaging guidance helps to remove residual tiny tumor tissues (Fig. 10d), while the generated ROS during post-surgery light treatment further contributes to ablate these remaining cancer cells. Such combination could effectively prolong the survival time of mice (Fig. 10e), which is promising for clinical practice of tumor resection surgery.

4. Antibacterial applications

Bacteria is a double-edged sword. It not only plays indispensable roles in various biological activities, but is also related to many diseases.[67] Bacterial infection is one of the fatal reasons of human death, but the detection and sterilization of harmful bacteria has always been a major challenge. PDT demonstrates a promising treatment modality for bacterial infection due to its high therapeutic specificity and non-invasive nature.[68] The development of AIE photosensitizers further promotes the photodynamic sterilization of bacteria, which has attracted widespread attention.[69–71] In this section, several different strategies to design light-up AIE probes for photodynamic antibacterial applications are discussed.

4.1. Physical binding mediated light-up probes

Based on the negatively charged nature of the bacterial surface, a large number of positively charged AIE probes have been developed.[72–74] Recently, Tang's group rationally developed a series of AIEgens (**TPy**, **TPPy**, **TTPy**, and **TPE-TTPy**) with continuously enhanced D–A structures for the detection and killing of Gram-positive bacteria (Fig. 11a).[75] Among these AIEgens, **TPy**, **TPPy**, and **TTPy** molecules can specifically recognize Gram-positive bacteria, but not for **TPE-TTPy**. This was attributed to the high hydrophobicity of **TPE-TTPy**. **TPE-TTPy** possesses the lowest critical aggregation concentration (1.8304 μM) and forms agglomerates during staining (the concentration is 2 μM) which has weak bacterial internalization (Fig. 11b). Different from **TPE-TTPy**, other molecules are more hydrophilic, so they can effectively label Gram-positive bacteria as molecular probes through a binding-mediated light-up feature. With an optimized D–A structure, **TTPy** showed extraordinary ROS production ability, which could induce an over 1000-fold fluorescence enhancement for ROS indicator dichlorofluorescin (DCFH) under white light irradiation, much higher than that of Chlorin **Ce6** (Fig. 11c). *In vitro* studies showed that **TTPy** could kill Gram-positive bacteria effectively under white light irradiation with a nearly 100% CFU reduction rate, showing its excellent antibacterial ability (Fig. 11d). *In vivo* *S. aureus*-infected wound healing studies further proved that **TTPy** could significantly inhibit bacterial infection of wounds

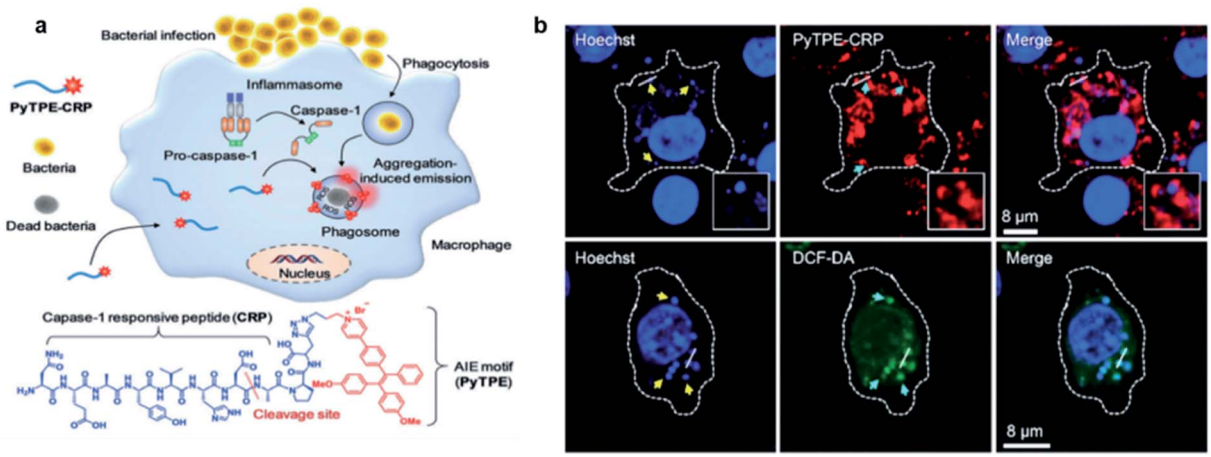

Fig. 12 (a) Schematic illustration of the macrophage-mediated intracellular bacterial infection diagnosis and elimination and the molecular structure of PyTPE-CRP. (b) Confocal images showing the localization of PyTPE-CRP inside *S. aureus* infected Raw 264.7 macrophages; confocal images of ROS detection inside the macrophages using DCF-DA generated by PyTPE-CRP. Reproduced from ref. 77 with permission. Copyright 2019 Wiley-VCH.

under PDT, leaving almost zero bacteria remaining in the soft tissue from infected sites (Fig. 11e and f).

4.2. Specific reaction mediated light-up probes

Although AIE probes based on electrostatic interactions have been widely developed, their selectivity can be greatly disturbed by the complex biological environment. Therefore, it is highly desirable to develop AIE light-up probes through specific chemical reaction. One of the successful approaches is to develop metabolic AIE probes to track and kill bacteria. Liu's group modified D-alanine with AIE photosensitizers, which could efficiently participate in the peptidoglycan metabolism of bacteria and show specific fluorescence light-up and photodynamic killing of targeted bacteria in both *in vitro* and *in vivo* studies.[76] Recently, the same group further reported a light-up probe for detection and killing of intracellular bacteria based on enzyme digestion strategies.[77] The AIE probe **PyTPE-CRP** was constructed by linking PyTPE to a casp-1 enzyme responsive peptide CRP (NEAYVHDAP) (Fig. 12a). **PyTPE-CRP** could be readily internalized into a macrophage and maintain fluorescence silence. The generation of the casp-1 enzyme inside the bacteria-infected macrophage could cleave CRP, leading to the aggregation of AIE residues with fluorescence turn-on. *In vitro* studies showed that **PyTPE-CRP** could light up macrophages infected with live *S. aureus* or *E. coli* but not for those infected with heat-inactivated bacteria, indicating that the probe serves the purpose well for real-time imaging of bacterial infection. Moreover, these **PyTPE-CRP** residues could accumulate at the phagosomes that contain bacteria and light-up these bacterial

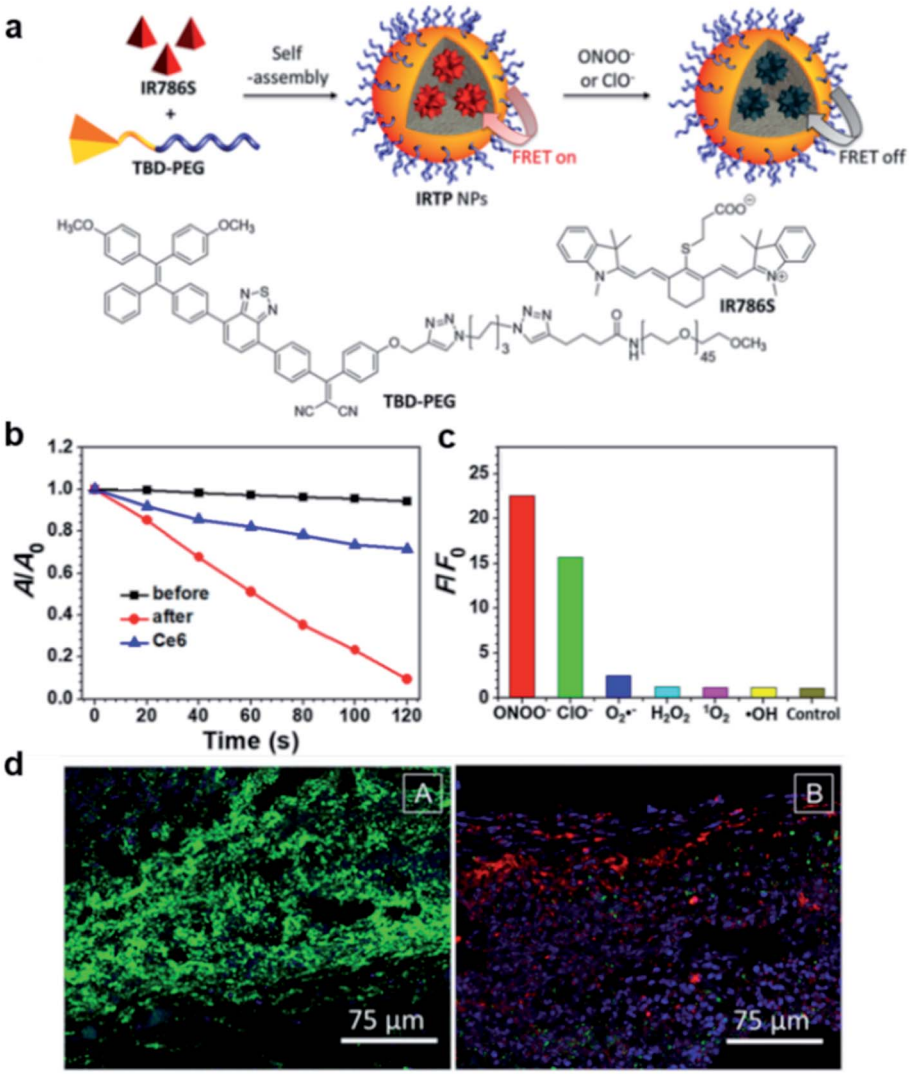

Fig. 13 (a) Schematic illustration of **IRTP** nanoparticle preparation. (b) The degradation rates of ABDA (50 μM) by **33%IRTP** NPs (20 μg mL^{-1} based on **TBD-PEG**) before and after $ONOO^-$ (140 μM) treatment; A_0 and A are the absorbance of ABDA in the presence of the nanoparticles at 378 nm before and after irradiation (60 mW cm^{-2}, 400–700 nm), respectively. (c) Fluorescence responses of **33%IRTP** nanoparticles toward different ROS; F and F_0 stand for the fluorescence intensities at 650 nm in the presence and absence of different ROS, respectively. (d) Fluorescence images of the GFP transgenic *E. coli* infected skin slices of mice treated with saline (left) or **33%IRTP** nanoparticles (right) for 6 h, followed by light irradiation treatment for 10 min. Reproduced from ref. 78 with permission. Copyright 2018 American Chemical Society.

phagosomes. Such accumulation leads to the precise ROS generation in these bacterial phagosomes without affecting the cells under light irradiation (Fig. 12b). Therefore, with AIE light-up probes, it becomes possible to sensitively detect bacterial infection and precisely eradiate intracellular bacteria.

Recently, a FRET system was applied to design light-up AIE probes for bacterial infection imaging and PDT.[78] The FRET system was constructed by encapsulation of an $ONOO^-$ and ClO^- responsive NIR dye (**IR786S**) using an amphiphilic AIE polymer (**TBD-PEG**) (Fig. 13a). Benefiting from the close interaction between the TBD core and **IR786S** and their matched emission–absorption spectra, the excited energy of **TBD-PEG** will be transferred to **IR786S**, leading to diminished fluorescence and ROS generation for **TBD-PEG**, but strong NIR emission for **IR786S**. It was found that 33% of **IR786S** was able to induce a complete FRET process, and the resultant nanoparticles (**33%IRTP**) were used for bacterial imaging and PDT applications. **IR786S** can be decomposed by $ONOO^-$ and ClO^-, and such decomposition could break the FRET process and restore the red fluorescence and ROS generation of **TBD-PEG** at the cost of **IR786S** emission (Fig. 13b). **33%IRTP** nanoparticles showed a very high responsive specificity towards $ONOO^-$ and ClO^- over other ROSs (Fig. 13c). As $ONOO^-$ and ClO^- are overexpressed in the bacteria-infected site, **33%IRTP** nanoparticles could hence be used for bacterial-infection imaging. Experimental results by transgenic green fluorescent protein *E. coli*-infected mice showed that **33%IRTP** nanoparticles were only activated at the site of bacterial infection, which was very beneficial for image-guided photodynamic bacterial ablation. As compared to the control group, light treatment after **33% IRTP** nanoparticles led to largely reduced *E coli* green fluorescence, which demonstrated the high efficiency of this FRET system for photodynamic antibacterial therapy (Fig. 13d).

5. Conclusion and perspectives

As a promising cancer treatment method, PDT has attracted widespread attention. The unique advantages of intensified emission and efficient photosensitization displayed in the aggregate state of AIEgens are particularly suitable for the development of light-up probes for image-guided PDT. In this review, we have discussed the recent advances of these AIE light-up probes in this field. D–A molecular engineering to reduce ΔE_{ST} is currently an effective method for designing high-efficiency photosensitizers, while the development of polymer photosensitizers and type-I photosensitizers has further expanded the AIE photosensitizer design. Based on the unique properties of the AIEgens, the control of molecular motions by aggregation or binding or reactions has become the unique and most commonly used design principle for AIE light-up probes. In addition, the traditional ways of realizing light-up by dequenching photophysical quenching processes are still applicable to AIEgens. Based on the above design principles, various AIE light-up probes have been developed for antitumor and antibacterial PDT applications.

Although AIE light-up probes have made significant progress in PDT, there are still many unresolved problems and challenges. Firstly, most AIE photosensitizers have a short excitation wavelength, which severely limits the depth of tissue penetration. The development of NIR-excited AIE photosensitizers is very necessary. Besides, multi-photon excitation and chemi-excitation provide PDT with deeper tissue penetration and more precise therapeutic accuracy, which could bring new windows for PDT. Secondly, the development of type-I AIE photosensitizers could largely improve PDT efficacy in the hypoxia tumor environment as they are less oxygen-dependent, which shall represent another promising direction for new AIE photosensitizer design. In addition, clinical treatment requires high accuracy and minimized side effects. More specific and selective light-up methods should be developed in order to completely overcome issues of false positives or false negatives. Apart from all of the above, studying the bio-distribution, long-term biocompatibility and pharmacokinetics of AIE probes in the body is crucial for future clinical translational work. We hope that this review will stimulate more interest of researchers from different disciplines to take the unique advantages of AIE to develop more specific and selective light-up probes to achieve more exciting advancements in PDT.

Conflicts of interest

There are no conflicts of interest to declare.

Acknowledgements

The authors thank the Singapore National Research Foundation (R279-000-483-281), National University of Singapore (R279-000-482-133), and Guangdong Provincial Key Laboratory of Luminescence from Molecular Aggregates (2019B030301003) for financial support.

Notes and references

1 C. M. Moore, D. Pendse and M. Emberton, *Nat. Clin. Pract. Urol.*, 2009, **6**, 18–30.
2 W. Fan, P. Huang and X. Chen, *Chem. Soc. Rev.*, 2016, **45**, 6488–6519.
3 E. M. Stennett, M. A. Ciuba and M. Levitus, *Chem. Soc. Rev.*, 2014, **43**, 1057–1075.
4 J. P. Celli, B. Q. Spring, I. Rizvi, C. L. Evans, K. S. Samkoe, S. Verma, B. W. Pogue and T. Hasan, *Chem. Rev.*, 2010, **110**, 2795–2838.
5 R. Bonnett, *Chem. Soc. Rev.*, 1995, **24**, 19–33.
6 B. M. Luby, C. D. Walsh and G. Zheng, *Angew. Chem., Int. Ed.*, 2019, **58**, 2558–2569.
7 W. Wu, X. Shao, J. Zhao and M. Wu, *Adv. Sci.*, 2017, **4**, 1700113.
8 J. Luo, Z. Xie, J. W. Lam, L. Cheng, H. Chen, C. Qiu, H. S. Kwok, X. Zhan, Y. Liu, D. Zhu and B. Z. Tang, *Chem. Commun.*, 2001, **18**, 1740–1741.
9 J. Mei, Y. Hong, J. W. Lam, A. Qin, Y. Tang and B. Z. Tang, *Adv. Mater.*, 2014, **26**, 5429–5479.
10 G. Feng and B. Liu, *Acc. Chem. Res.*, 2018, **51**, 1404–1414.

11 D. Wang and B. Z. Tang, *Acc. Chem. Res.*, 2019, **52**, 2559–2570.
12 F. Hu, S. Xu and B. Liu, *Adv. Mater.*, 2018, **30**, e1801350.
13 G. Feng, G. Q. Zhang and D. Ding, *Chem. Soc. Rev.*, 2020, **49**, 8179–8234.
14 J. Zhao, W. Wu, J. Sun and S. Guo, *Chem. Soc. Rev.*, 2013, **42**, 5323–5351.
15 C. Adachi, M. A. Baldo, M. E. Thompson and S. R. Forrest, *J. Appl. Phys.*, 2001, **90**, 5048–5051.
16 C. A. Robertson, D. H. Evans and H. Abrahamse, *J. Photochem. Photobiol., B*, 2009, **96**, 1–8.
17 C. Chen, X. Ni, H. W. Tian, Q. Liu, D. S. Guo and D. Ding, *Angew. Chem., Int. Ed.*, 2020, **59**, 10008–10012.
18 C. Chen, H. Ou, R. Liu and D. Ding, *Adv. Mater.*, 2020, **32**, 1806331.
19 A. Kamkaew, S. H. Lim, H. B. Lee, L. V. Kiew, L. Y. Chung and K. Burgess, *Chem. Soc. Rev.*, 2013, **42**, 77–88.
20 C. M. Marian, *Wiley Interdiscip. Rev.: Comput. Mol. Sci.*, 2012, **2**, 187–203.
21 C. Zhang, Y. Zhao, D. Li, J. Liu, H. Han, D. He, X. Tian, S. Li, J. Wu and Y. Tian, *Chem. Commun.*, 2019, **55**, 1450–1453.
22 W. Wu, D. Mao, S. Xu, S. Ji, F. Hu, D. Ding, D. Kong and B. Liu, *Mater. Horiz.*, 2017, **4**, 1110–1114.
23 S. Xu, W. Wu, X. Cai, C. J. Zhang, Y. Yuan, J. Liang, G. Feng, P. Manghnani and B. Liu, *Chem. Commun.*, 2017, **53**, 8727–8730.
24 W. Wu, D. Mao, F. Hu, S. Xu, C. Chen, C. J. Zhang, X. Cheng, Y. Yuan, D. Ding, D. Kong and B. Liu, *Adv. Mater.*, 2017, **29**, 1110–1114.
25 W. Wu, D. Mao, S. Xu, Kenry, F. Hu, X. Li, D. Kong and B. Liu, *Chem*, 2018, **4**, 1937–1951.
26 S. Liu, H. Zhang, Y. Li, J. Liu, L. Du, M. Chen, R. T. K. Kwok, J. W. Y. Lam, D. L. Phillips and B. Z. Tang, *Angew. Chem., Int. Ed.*, 2018, **57**, 15189–15193.
27 E. Ju, K. Dong, Z. Chen, Z. Liu, C. Liu, Y. Huang, Z. Wang, F. Pu, J. Ren and X. Qu, *Angew. Chem., Int. Ed.*, 2016, **55**, 11467–11471.
28 Z. Yang, Y. Dai, C. Yin, Q. Fan, W. Zhang, J. Song, G. Yu, W. Tang, W. Fan, B. C. Yung, J. Li, X. Li, X. Li, Y. Tang, W. Huang, J. Song and X. Chen, *Adv. Mater.*, 2018, **30**, 1707509.
29 M. Huo, L. Wang, Y. Chen and J. Shi, *Nat. Commun.*, 2017, **8**, 357.
30 Z. Zhuang, J. Dai, M. Yu, J. Li, P. Shen, R. Hu, X. Lou, Z. Zhao and B. Z. Tang, *Chem. Sci.*, 2020, **11**, 3405–3417.
31 Q. Wan, R. Zhang, Z. Zhuang, Y. Li, Y. Huang, Z. Wang, W. Zhang, J. Hou and B. Z. Tang, *Adv. Funct. Mater.*, 2020, **30**, 2002057.
32 J. Dai, Y. Li, Z. Long, R. Jiang, Z. Zhuang, Z. Wang, Z. Zhao, X. Lou, F. Xia and B. Z. Tang, *ACS Nano*, 2020, **14**, 854–866.
33 T. Zhou, R. Hu, L. Wang, Y. Qiu, G. Zhang, Q. Deng, H. Zhang, P. Yin, B. Situ, C. Zhan, A. Qin and B. Z. Tang, *Angew. Chem., Int. Ed.*, 2020, **59**, 9952–9956.
34 J. S. Ni, T. Min, Y. Li, M. Zha, P. Zhang, C. L. Ho and K. Li, *Angew. Chem., Int. Ed.*, 2020, **59**, 10179–10185.
35 X. Ni, X. Zhang, X. Duan, H. L. Zheng, X. S. Xue and D. Ding, *Nano Lett.*, 2019, **19**, 318–330.
36 J. Liang, B. Z. Tang and B. Liu, *Chem. Soc. Rev.*, 2015, **44**, 2798–2811.
37 Y. Gao, X. Wang, X. He, Z. He, X. Yang, S. Tian, F. Meng, D. Ding, L. Luo and B. Z. Tang, *Adv. Funct. Mater.*, 2019, **29**, 1902673.
38 R. Kumar, W. S. Shin, K. Sunwoo, W. Y. Kim, S. Koo, S. Bhuniya and J. S. Kim, *Chem. Soc. Rev.*, 2015, **44**, 6670–6683.
39 J. Shi, Y. Li, Q. Li and Z. Li, *ACS Appl. Mater. Interfaces*, 2018, **10**, 12278–12294.
40 Y. Yuan, C. J. Zhang, M. Gao, R. Zhang, B. Z. Tang and B. Liu, *Angew. Chem., Int. Ed.*, 2015, **54**, 1780–1786.
41 L. Yuan, W. Lin, K. Zheng and S. Zhu, *Acc. Chem. Res.*, 2013, **46**, 1462–1473.
42 D. Escudero, *Acc. Chem. Res.*, 2016, **49**, 1816–1824.
43 Y. Tang, D. Lee, J. Wang, G. Li, J. Yu, W. Lin and J. Yoon, *Chem. Soc. Rev.*, 2015, **44**, 5003–5015.
44 C. Zhan, G. Zhang and D. Zhang, *ACS Appl. Mater. Interfaces*, 2018, **10**, 12141–12149.
45 F. Hu, Y. Huang, G. Zhang, R. Zhao, H. Yang and D. Zhang, *Anal. Chem.*, 2014, **86**, 7987–7995.
46 D. Wang, H. Su, R. T. K. Kwok, X. Hu, H. Zou, Q. Luo, M. M. S. Lee, W. Xu, J. W. Y. Lam and B. Z. Tang, *Chem. Sci.*, 2018, **9**, 3685–3693.
47 J. Morgan and A. R. Oseroff, *Adv. Drug Delivery Rev.*, 2001, **49**, 71–86.
48 W. Lv, Z. Zhang, K. Y. Zhang, H. Yang, S. Liu, A. Xu, S. Guo, Q. Zhao and W. Huang, *Angew. Chem., Int. Ed.*, 2016, **55**, 9947–9951.
49 S. Fulda, L. Galluzzi and G. Kroemer, *Nat. Rev. Drug Discovery*, 2010, **9**, 447–464.
50 C. Gui, E. Zhao, R. T. K. Kwok, A. C. S. Leung, J. W. Y. Lam, M. Jiang, H. Deng, Y. Cai, W. Zhang, H. Su and B. Z. Tang, *Chem. Sci.*, 2017, **8**, 1822–1830.
51 M. Jiang, R. T. K. Kwok, X. Li, C. Gui, J. W. Y. Lam, J. Qu and B. Z. Tang, *J. Mater. Chem. B*, 2018, **6**, 2557–2565.
52 G. Feng, J. Liu, C. J. Zhang and B. Liu, *ACS Appl. Mater. Interfaces*, 2018, **10**, 11546–11553.
53 C. Chen, X. Ni, S. Jia, Y. Liang, X. Wu, D. Kang and D. Ding, *Adv. Mater.*, 2019, **31**, 1904914.
54 W. Xu, M. M. S. Lee, J. J. Nie, Z. Zhang, R. T. K. Kwok, J. W. Y. Lam, F. J. Xu, D. Wang and B. Z. Tang, *Angew. Chem., Int. Ed.*, 2020, **59**, 9610–9616.
55 J. Dai, C. Duan, Y. Huang, X. Lou, F. Xia and S. Wang, *J. Mater. Chem. B*, 2020, **8**, 3357–3370.
56 F. Li, Y. Du, J. Liu, H. Sun, J. Wang, R. Li, D. Kim, T. Hyeon and D. Ling, *Adv. Mater.*, 2018, **30**, 1802808.
57 D. Cui, J. Huang, X. Zhen, J. Li, Y. Jiang and K. Pu, *Angew. Chem., Int. Ed.*, 2019, **58**, 5920–5924.
58 S. Ji, H. Gao, W. Mu, X. Ni, X. Yi, J. Shen, Q. Liu, P. Bao and D. Ding, *J. Mater. Chem. B*, 2018, **6**, 2566–2573.
59 M. H. Lee, Z. Yang, C. W. Lim, Y. H. Lee, S. Dongbang, C. Kang and J. S. Kim, *Chem. Rev.*, 2013, **113**, 5071–5109.
60 F. Hu, Y. Yuan, D. Mao, W. Wu and B. Liu, *Biomaterials*, 2017, **144**, 53–59.
61 L. Shao, Y. Pan, B. Hua, S. Xu, G. Yu, M. Wang, B. Liu and F. Huang, *Angew. Chem., Int. Ed.*, 2020, **59**, 11779–11783.

62 R. Rossin, P. R. Verkerk, S. M. van den Bosch, R. C. Vulders, I. Verel, J. Lub and M. S. Robillard, *Angew. Chem., Int. Ed.*, 2010, **49**, 3375–3378.
63 N. K. Devaraj, *ACS Central Science*, 2018, **4**, 952–959.
64 S. S. Nguyen and J. A. Prescher, *Nat. Rev. Chem.*, 2020, **4**, 476–489.
65 F. Hu, D. Mao, Kenry, X. Cai, W. Wu, D. Kong and B. Liu, *Angew. Chem., Int. Ed.*, 2018, **57**, 10182–10186.
66 J. Qi, C. Chen, X. Zhang, X. Hu, S. Ji, R. T. K. Kwok, J. W. Y. Lam, D. Ding and B. Z. Tang, *Nat. Commun.*, 2018, **9**, 1848.
67 N. D. Wolfe, C. P. Dunavan and J. Diamond, *Nature*, 2007, **447**, 279–283.
68 Y. Liu, R. Qin, S. A. J. Zaat, E. Breukink and M. Heger, *J. Clin. Transl. Res.*, 2015, **1**, 140–167.
69 G. Feng, Y. Yuan, H. Fang, R. Zhang, B. Xing, G. Zhang, D. Zhang and B. Liu, *Chem. Commun.*, 2015, **51**, 12490–12493.
70 X. He, L. H. Xiong, Z. Zhao, Z. Wang, L. Luo, J. W. Y. Lam, R. T. K. Kwok and B. Z. Tang, *Theranostics*, 2019, **9**, 3223–3248.
71 J. Zhuang, H. Yang, Y. Li, B. Wang, N. Li and N. Zhao, *Chem. Commun.*, 2020, **56**, 2630–2633.
72 G. Feng, C. J. Zhang, X. Lu and B. Liu, *ACS Omega*, 2017, **2**, 546–553.
73 X. Liu, Z. Yang, W. Xu, Y. Chu, J. Yang, Y. Yan, Y. Hu, Y. Wang and J. Hua, *J. Mater. Chem. C*, 2019, **7**, 12509–12517.
74 B. Ren, K. Li, Z. Liu, G. Liu and H. Wang, *J. Mater. Chem. B*, 2020, **8**, 10754–10763.
75 M. Kang, C. Zhou, S. Wu, B. Yu, Z. Zhang, N. Song, M. M. S. Lee, W. Xu, F. J. Xu, D. Wang, L. Wang and B. Z. Tang, *J. Am. Chem. Soc.*, 2019, **141**, 16781–16789.
76 D. Mao, F. Hu, Kenry, G. Qi, S. Ji, W. Wu, D. Kong and B. Liu, *Mater. Horiz.*, 2020, **7**, 1138–1143.
77 G. Qi, F. Hu, Kenry, L. Shi, M. Wu and B. Liu, *Angew. Chem., Int. Ed.*, 2019, **58**, 16229–16235.
78 W. Wu, D. Mao, X. Cai, Y. Duan, F. Hu, D. Kong and B. Liu, *Chem. Mater.*, 2018, **30**, 3867–3873.